

Magnetotransport in polycrystalline $\text{La}_{2/3}\text{Sr}_{1/3}\text{MnO}_3$ thin films of controlled granularity

P. K. Muduli, Gyanendra Singh, R. Sharma, R. C. Budhani*

*Condensed Matter - Low Dimensional Systems Laboratory, Department of Physics,
Indian Institute of Technology Kanpur, Kanpur - 208016, India*

(Dated: November 7, 2018)

arXiv:0905.1306v1 [cond-mat.str-el] 8 May 2009

Abstract

Polycrystalline $\text{La}_{2/3}\text{Sr}_{1/3}\text{MnO}_3$ (LSMO) thin films were synthesized by pulsed laser ablation on single crystal (100) yttria-stabilized zirconia (YSZ) substrates to investigate the mechanism of magneto-transport in a granular manganite. Different degrees of granularity is achieved by using the deposition temperature (T_D) of 700 and 800 $^{\circ}\text{C}$. Although no significant change in magnetic order temperature (T_C) and saturation magnetization is seen for these two types of films, the temperature and magnetic field dependence of their resistivity ($\rho(T, H)$) is strikingly dissimilar. While the $\rho(T, H)$ of the 800 $^{\circ}\text{C}$ film is comparable to that of epitaxial samples, the lower growth temperature leads to a material which undergoes insulator-to-metal transition at a temperature ($T_P \approx 170$ K) much lower than T_C . At $T \ll T_P$, the resistivity is characterized by a minimum followed by $\ln T$ divergence at still lower temperatures. The high negative magnetoresistance ($\approx 20\%$) and $\ln T$ dependence below the minimum are explained on the basis of Kondo-type scattering from blocked Mn-spins in the intergranular material. Further, a striking feature of the $T_D = 700$ $^{\circ}\text{C}$ film is its two orders of magnitude larger anisotropic magnetoresistance (AMR) as compared to the AMR of epitaxial films. We attribute it to unquenching of the orbital angular momentum of 3d electrons of Mn ions in the intergranular region where crystal field is poorly defined.

PACS numbers: XX-XX, XX-XX-XX

I. INTRODUCTION

Low field magnetoresistance (LFMR) in half-metallic granular systems has attracted considerable scientific interest because of the physics of spin-polarized tunneling which encompasses several energy scales, as well as its potential technological applications. Polycrystalline thin films of magnetite¹, chromium dioxide², manganites^{3,4,5,6} and double perovskites^{7,8,9} are the most studied systems of this class. It has also been shown that the magnetoresistive properties of granular ferromagnetic metals can change significantly due to spin-dependent scattering at the grain boundaries¹⁰. However, the grain boundary magnetoresistance in manganites may be different from the magnetoresistance (MR) of granular band ferromagnets such as Fe, Co and Ni. In the former case, the magnetic structure at the surface of grains is likely to be chaotic with blocked Mn-spins. This is because of the propensity of surfaces to loose oxygen which can render the double exchange interaction, the source of magnetism and metallic conduction in these systems, weaker at the surfaces and interfaces. Therefore, beside the usual tunneling through insulating barriers, second order tunneling encompassing interfacial spins at the grain boundaries may be important in setting the MR of granular manganites^{3,11}. Furthermore, when the granules are small,

the Coulomb charging energy may also be a relevant energy scale at low-temperatures. The intergranular Coulomb blockade scenario has been invoked in some cases to understand the low-temperature upturn in the resistivity of granular manganites^{12,13,14}. The validity of such a hypothesis, however, needs to be examined by looking for voltage threshold for conduction and non-linear transport, which are important hallmarks of Coulomb blockade.

Another important issue concerning the MR in granular manganites is the anisotropic magnetoresistance (AMR). The AMR in clean double exchange manganites has many contrasting features compared to that in transition metal ferromagnets and alloys where it is firmly believed to be due to spin-orbit interaction. In most conventional metallic ferromagnets, the resistivity ρ_{\perp} is found to be smaller than ρ_{\parallel} and AMR decreases on approaching the T_C , where ρ_{\parallel} and ρ_{\perp} denotes the resistivity for magnetic field parallel and perpendicular to the current respectively. In contrast, manganites typically display the inequality $\rho_{\parallel} < \rho_{\perp}$. Also, the AMR is weakly temperature dependent, except for a peak near the Curie temperature T_C ^{15,16,17}. While a common mechanism may be responsible for the high-field AMR in single crystal and polycrystalline manganites, at low fields AMR of the latter may contain extrinsic contribution originating from grain boundary magnetization anisotropy.

Furthermore, since the peak in temperature dependence of AMR of manganites has been explained in terms of the unquenching of orbital moments due to the enhanced Jahn-Teller (JT) distortions near T_C ¹⁸, an enhanced AMR effect is expected in polycrystalline samples where double exchange is suppressed at the grain boundaries making JT electron-lattice coupling more relevant.

Here we report a detail study of both low-field magnetoresistance and anisotropic magnetoresistance in thin films of $\text{La}_{2/3}\text{Sr}_{1/3}\text{MnO}_3$ (LSMO), the most promising manganite for room temperature applications. These films were deposited using an excimer laser based pulsed laser ablation technique on single crystal (100) yttria-stabilized zirconia (YSZ) and (100) SrTiO_3 (STO) substrates. Also different deposition temperatures ($T_D = 700$ and 800 °C) were used to control the granular texture of the films. The crystalline quality and surface morphology were well characterized through X-ray diffraction and atomic force microscopy (AFM) techniques. The effect of granularity on magnetic nature of the films was also analyzed by observing the temperature and field dependence of magnetization. A phenomenological model was introduced to explain the temperature dependent resistivity in case of polycrystalline films deposited at the lower temperature. The films were presumed

to be a two-component medium with ferromagnetic metallic intragrain and spin-glass-type dirty intergrain metal. The low-temperature up-turn in the resistivity was found to scale as $\rho \sim \ln T$ representing a Kondo-type behavior in the dirty metal. The large anisotropic magnetoresistance (AMR) were explained through spin-orbit coupling and grain boundary effects.

II. EXPERIMENTAL PROCEDURE

Thin films of LSMO were fabricated by Pulsed Laser Deposition (PLD) method as described in detail elsewhere¹⁹. A KrF excimer laser (wavelength $\lambda = 248$ nm and pulse width ≈ 20 nanosecond) was used for ablation. Films of typically 100 nm in thickness were grown on (100) SrTiO₃ (STO) and (100) yttria-stabilized zirconia (YSZ) substrates in the temperature (T_D) range of 700 to 800 °C in 0.4 mbar oxygen pressure. A growth rate of ≈ 1.3 Å/sec was realized by firing the laser at 5 Hz with fluency of ~ 3 J/cm²/pulse on the target surface. After deposition, the films were cooled down to room temperature at the rate of 10 °C/min under an atmospheric oxygen pressure. The surface morphology of the films was examined using an atomic force microscope (AFM) where as for their crystallographic structure we have used a X-ray diffractometer (PANalytical X'Pert PRO) equipped with a Cu

$K_{\alpha 1}$ source. For electrical measurements, samples were patterned in a four-probe geometry with effective area of $200 \mu\text{m} \times 1000 \mu\text{m}$ using optical lithography and Ar^+ ion milling. The resistivity and magnetoresistance measurements were performed in a constant current mode using a precision programmable DC current source (Keithley 224), a temperature controller (Lakeshore 311) and a nanovoltmeter (HP 34420 A nanovolt/micro-ohm meter). For the measurements of magnetization, we have used a superconducting quantum interference device (SQUID) based magnetometer (Quantum Design MPMS-XL5).

III. RESULTS AND DISCUSSION

A. Microstructural properties

We first quantify the extent of granularity in our films using X-ray diffraction and AFM techniques. Polycrystalline nature of the LSMO films grown on YSZ at 700 and 800 °C becomes clear from the diffraction profiles shown in Fig. 1(a) and (b) respectively. Although the lattice parameter of YSZ ($a_{\text{YSZ}} = 0.514 \text{ nm}$) is very large compared to that of LSMO ($a_{\text{LSMO}} = 0.388 \text{ nm}$), the face diagonal of LSMO cubic cell is only 6.7 % shorter than a_{YSZ} , which should facilitate a preferential (110) oriented growth on (100) YSZ substrate. However, the $\theta - 2\theta$ scan shown in Fig. 1 reveals the presence of (001), (0kl) and (hkl)

reflections in addition to (hk0), confirming a truly polycrystalline growth. We also note that the X-ray intensity ratio $I(002)/I(110)$ for film deposited at 700 and 800 °C is ≈ 0.14 and ≈ 2.99 respectively. The smaller value of the ratio in case of films deposited at the lower temperature imply more random texture as compared to that in the film deposited at 800 °C²⁰.

The surface morphology of films deposited at 700 and 800 °C is shown in Fig. 2(a) and (b) respectively. The AFM image of the film with $T_D = 800$ °C shows granular morphology with spherical grains of average diameter ≈ 50 nm. The film with $T_D = 700$ °C is seen to contain ellipsoidal grains with average length ≈ 80 nm and width ≈ 30 nm. The rms roughness of the films was found out to be ≈ 8.59 nm and ≈ 7.85 nm over an area of 5×5 μm^2 for film deposited at 700 and 800 °C respectively.

B. Electrical resistivity and its temperature and magnetic field dependence

Epitaxial films of LSMO are characterized by metallic conduction with a low (≈ 110 $\mu\Omega\text{-cm}$) residual resistivity¹⁹. Interestingly, unlike the other double-exchange manganites the conduction in LSMO remains metallic even at temperatures greater than the magnetic ordering temperature(T_C)^{21,22,23}. In Fig. 3(a) we show the $\rho(T)$ in the temperature range

of 10-300 K of a LSMO film deposited on SrTiO₃. The temperature dependence seen here is consistent with the canonical behavior stated in the preceding line. Interestingly, the polycrystalline films deposited at 800 °C on YSZ also shows a similar behavior, although with a higher overall resistivity, which can be attributed to grain boundary scattering in a homogeneous polycrystalline film. The temperature dependence of resistivity in metallic LSMO is given by²⁴

$$\rho(T) = \rho_1 + AT^2 + A_{4.5}T^{4.5}, \quad (1)$$

where ρ_1 is the residual temperature-independent resistivity due to scattering by impurities and defects. The second term in Eq. (1) is due to electron-electron scattering, and third term describes the second order electron-magnon scattering²⁴. The parameters extracted by fitting Eq. (1) to the data of Fig. 3(a) are listed in the Table 1 and they match well with the values reported in literature^{24,25}. The temperature dependence of the field-cooled (FC) magnetization $M(T)$ measured at 100 Oe of the film deposited at 800 °C on YSZ is shown in the inset of Fig. 3(a). The magnetization near the Curie temperature goes to zero as $M(T) \sim (T-T_C)^\beta$, with $\beta \approx 0.38 \pm 0.01$ and $T_C \approx 350$ K. The critical exponent β compares well with the value ($\approx 0.37 \pm 0.04$) for single crystal La_{2/3}Sr_{1/3}MnO₃²⁶. In the

same inset we also plot the FC magnetization of a film deposited at 700 °C on YSZ. While the magnetic ordering temperature T_C of the 700 and 800 °C deposited films is nearly the same, a remarkably different temperature dependence of resistivity emerges for the former, as shown in Fig. 3(b). The $\rho(T)$ is now thermally activated down to T_P and then a metallic behavior develops in the temperature window of 170 - 50 K followed by reentry into a semiconducting regime at still lower temperatures. The resistivity of these films at $T \leq T_P$ also drops significantly on application of a small magnetic field with a concomitant shift of T_P to higher temperatures as shown in the inset of Fig. 3(b).

We now examine the $\rho(T)$ data of Fig. 3(b) in the light of structural and topographical information. Our AFM results clearly indicate a two-component medium where well formed but randomly oriented grains of LSMO are separated by an intergranular material, which is presumed to be a dirty ferromagnetic metal with a range of magnetic ordering temperatures lower than the T_C of bulk LSMO. A depression in T_C of large bandwidth manganites such as LSMO due to distortion in bond angles and bond lengths, and oxygen deficiency is well established experimentally^{27,28}. Such deviations from the ideal structure are common at the surfaces of grains in transition metal oxides^{5,29}. A pictorial view of our model is presented

in Fig. 4. We divide the resistivity curve into three zones. In the Zone-1 ($T_P < T < T_C$), we have nanometer scale (≈ 80 nm) ferromagnetic granules of the Curie temperature T_C^G (≈ 350 K) embedded in a paramagnetic insulator. This is the intergranular material with a magnetic ordering temperature $T^{IG}_C \approx T_P$, which is consistent with the observation that the T_C of LSMO can be reduced significantly by oxygen deficiency and disorder^{27,28}. Then comes Zone-2 of temperature ($T_{min} < T \leq T_P$) where the intergranular disordered LSMO is a dirty metal with ferromagnetic ordering. Finally in the Zone-3 ($T \leq T_{min}$) Kondo-type scattering from the blocked Mn-spins in the intergranular dirty ferromagnet leads to the divergence of resistivity on cooling below T_{min} .

We now discuss electron transport in each of these regimes in detail and augment this intuitive model with more data. The resistivity in Zone-1 is thermally activated but with a negligibly small temperature dependent activation energy, suggesting phonon mediated variable range tunneling through the paramagnetic insulator. The insignificant field dependence of resistivity in Zone-1 [see Fig. 3(b)] can be attributed to spin-flip scattering of spin-polarized holes as they move between two neighboring clusters via hopping through the localized states of the paramagnetic insulator where each localizing state has a moment

(Mn^{3+} polaron with $S = 3/2$). The spin-flip scattering does not permit a spin-selective transport between two ferromagnetic grains, which is essential for large magnetoresistance (MR). In magnetically inactive insulating media such as SiO_2 , Al_2O_3 , MgO etc. where spin-selectivity is not blocked, one, however, sees a large MR. Typical examples of such system are cermet film like Ni-SiO_2 , Co-SiO_2 and Fe-SiO_2 etc.^{10,30,31,32}

We argue that in the vicinity of $T \approx T_P$, a sufficient fraction of the intergranular material undergoes magnetic ordering to a ferromagnetic phase. Like other double exchange manganites, the ordered phase is presumably metallic with a large value of resistivity, which is consistent with observed inverse scaling between $\rho(0)$ and T_C of the manganites^{21,22}. The large magnetoresistance near T_P and the shift of T_P to higher temperatures on increasing the field are also consistent with this picture of a PM to FM transition accompanied by a transition in electrical conductivity. In the metallic regime (Zone-2 of Fig. 4(c)), the system can be viewed as a microscopic mixture of two materials, grain G and intergranular IG, with respective resistivity ρ_G and ρ_{IG} . The temperature dependence is dominated entirely by intrinsic transport in the more resistive intergranular dirty metal. We believe that tunneling dominated transport, as argued by some workers for polycrystalline films of LSMO,

is unlikely to occur in such cases because one does not see a Coulomb blockade regime in current-voltage characteristics even at fairly low-temperatures (5 K) which remain linear even at very small bias voltages. It is worth pointing out that electron transport in granular manganites has often been compared with the data on thin films of insulating matrix system such as Co-SiO₂, Ni-SiO₂ and Ni-SiO₂. The resistivity of such systems at low-temperature varies as^{10,30,31,32};

$$\rho = \rho_0 \exp\left(\frac{T_0}{T}\right)^{1/2}, \quad (2)$$

where the exponential factor T_0 depends on the electrostatic charging energy of the metallic grains (Ni or Co), width of tunneling barrier and the barrier height. These systems, however, do not show the type of metallic behavior seen in Zone-2 of Fig. 4(c).

In Fig. 5(a) we plot the semiconductor-like resistivity of Zone-3 as a function of $T^{-1/2}$. For zero-field case the value of T_0 is found to be ≈ 1.07 K (0.09 meV). However, a calculation based on the charging energy $E_C = e^2/2C$, with $C = 4\pi\epsilon_0\epsilon r$, $r \approx 80$ nm and $\epsilon \approx 10$ gives $E_C \approx 0.9$ meV, which is an order of magnitude larger than T_0 . Although T_0 also depends on barrier width and height, such large mismatch in measured T_0 and calculated E_C cannot be accounted for with admissible variations in barrier height and its width. In the following,

we argue that the transport in Zone-3 is not due to ballistic tunneling through a clean wide-band-gap insulator like SiO_2 or Al_2O_3 as in cermet films, but a consequence of Kondo-type scattering in the intergranular spin-disordered dirty metal.

To understand the temperature dependence of resistivity in more detail one can consider a two-component system whose effective resistivity is given by the effective medium approximation^{33,34} as

$$f \left(\frac{\rho_M - \rho_{eff}}{2\rho_M + \rho_{eff}} \right) + (1 - f) \left(\frac{\rho_{DM} - \rho_{eff}}{2\rho_{DM} + \rho_{eff}} \right) = 0. \quad (3)$$

Here f represents the volume fraction of clean ferromagnetic metallic regions whose resistivity is ρ_M [the grains] and $(1-f)$ the dirty ferromagnetic metal of intergrain space having resistivity ρ_{DM} . However we have used a simpler approach where the clean and dirty metallic regions are connected in series. The effective resistivity is written as;

$$\rho_{eff} = f\rho_M + (1 - f)\rho_{DM}. \quad (4)$$

We assume that the semiconducting behavior in Zone-3 is either due to electron-electron (e-e) interaction or due to Kondo-scattering in the small $(1-f)$ fraction of the intergranular

dirty metal. In the e-e interaction picture, the resistivity is given by³⁵

$$\rho_{DM} = \rho_2(1 - BT^{1/2}) \quad (5)$$

where ρ_2 is the residual resistivity contributed by temperature independent scattering processes and B a constant with value in the range of $5 - 20 \times 10^{-4} \text{ K}^{-1/2}$ for disordered alloys. Substituting Eqs. (5) and (1) into Eq. (4), we find

$$\rho_{eff} = f\rho_1 + fAT^2 + fA_{4.5}T^{4.5} + (1 - f)\rho_2 + \rho_2(f - 1)BT^{1/2} \quad (6)$$

A best fit of the data in Zone-3 to Eq. (6) is displayed in Fig. 5(b). The constants A and $A_{4.5}$ for the fit were taken from the data on epitaxial LSMO thin film as listed in Table 1. Furthermore, the metallic fraction has been set at $f \approx 0.9$ by analyzing the AFM images of the polycrystalline film (ellipsoidal grains with $a \approx b \approx 30 \text{ nm}$ and $c \approx 80 \text{ nm}$ with a grain boundary thickness of $\sim 1 \text{ nm}$). However, even with such reasonable choices of ρ_1 , A , $A_{4.5}$ and f , poor quality of fit obtained suggests that the electron-electron interaction picture may not be appropriate to explain the low-temperature behavior of $\rho(T)$.

In an alternative approach considering a Kondo-type behavior of resistivity in the dirty

ferromagnetic metal, we can write³⁶

$$\rho_{DM} = \rho_3 + \delta T^2 + \gamma \ln T \quad (7)$$

Where ρ_3 is the temperature independent residual resistivity and the T^2 term is due to electron-electron scattering as observed in typical metals. The third term with coefficient γ corresponds to the Kondo-type scattering process, which in the present case will be due to disordered Mn-spins. From Eq. (7) we can write the temperature corresponding to resistivity minimum as;

$$T_m = \left(-\frac{\gamma}{2\delta} \right)^{1/2}. \quad (8)$$

Substituting Eq. (7) and Eq. (1) into Eq. (4), and rearranging the coefficients the effective resistivity can be written as;

$$\rho_{eff} = \alpha + f\rho_1 + fAT^2 + fA_{4.5}T^{4.5} + (1-f)\delta T^2 + (1-f)\gamma \ln T, \quad (9)$$

where the constant $\alpha (= (1-f)\rho_3)$ depends on the residual resistivity of the intergranular dirty metal. A fitting of Eq. (9) to the experimental data in the temperature range 50 to 5 K is shown in Fig. 5(c) with fixed ρ_1 , f , A and $A_{4.5}$ derived from $\rho(T)$ of epitaxial films and AFM images shown in Fig. 2(a). The fitting parameters for different field in the

temperature range 50 to 10 K are listed in Table. 1. The resistivity minimum temperature T_m calculated using Eq. (8) is 52.2 K. The larger value of parameter δ compared to that of A is due to the fact that A increases rapidly with oxygen deficiency and strain. This become clear from the order of magnitude larger value of A in film deposited on YSZ at 800 $^{\circ}\text{C}$ compared to those on STO of the same T_D . The films on YSZ are polycrystalline and likely to have oxygen deficiency at the grain boundaries.

To understand the effect of magnetic field, the temperature dependent resistivity measured at different fields is also fitted to Eq. (9). The best fit to the data taken at 0.3 T is shown in Fig. 5(c). The coefficient γ of the $\ln T$ term in Eq. (7) calculated from the fitting is shown in Fig. 5(d). The negative sign of the coefficient γ is consistent with a Kondo-type picture. Thus application of magnetic field suppresses spin- disorder and hence spin-dependent-scattering and leads to negative magnetoresistance.

To understand the origin of magnetoresistance further, particularly in a low field regime where moment of the grains are not fully aligned, we look at the correlation between isothermal magnetization and low-field magnetoresistance of these films in the temperature regime corresponding to Zone-3. A typical set of data taken at 20 K for the samples deposited

at 700 and 800 ⁰ C acquired in a configuration where field and current are coplanar but orthogonal to each other is shown in Fig. 6. The MR has been defined as;

$$MR(\%) = \frac{R(H) - R(0)}{R(0)} \times 100, \quad (10)$$

where R(H) and R(0) are resistances in the presence of field and in zero-field respectively.

The MR is initially positive and increases with field, peaking for a field of H_P (≈ 222 Oe).

On increasing the field beyond H_P, the MR becomes negative and reaches a value ≈ 19 %

for a small field of 0.3 T. However, initial ~ 70 % of the drop in resistance occurs for field

H ≤ 0.15 T followed by a linear increase at higher fields. The MR in these films were found

out to be symmetric for both positive and negative field direction. The hysteresis in MR can

also be understood considering the fact that for lower fields the magnetization vector (**M**) of

individual grains are aligned along their easy axis and for field higher than H_C the grains get

aligned along the field direction resulting in a parallel low resistance state³⁷. In Fig. 6 we

have also plotted the field dependence of magnetization to emphasize the correlation between

coercive field (H_C) and the field (± H_P) at which MR shows peaks on field reversal. We

notice that while for the films with T_D= 800 ⁰C, H_P ≈ H_C, where as in the film deposited at

$700\text{ }^{\circ}\text{C}$ $H_P > H_C$. Similar inequality has also been seen in other polycrystalline half-metallic perovskite oxides like $\text{Sr}_2\text{FeMoO}_6$ (SFMO)⁸. The distinctive feature in the present case is that the intergrain material is a spin-disordered dirty metal. However, the small mismatch ($\sim 100\text{ Oe}$) between H_P and H_C can also be understood by considering the fact that in MR measurement the current circulates only a fraction of the magnetic grains which fall on the percolating path whereas the magnetization is a bulk measurement which reflects the average response of the whole sample³⁸. The $800\text{ }^{\circ}\text{C}$ deposited sample showed a better H_C vs H_P matching may be due to better connectivity between grains therefore a larger fraction of the sample contributes to the MR measurement.

C. Anisotropic magnetoresistance (AMR)

Although the anisotropy in magnetoresistance seen in ferromagnetic metals may have different origin involving increased pathlength due to the Lorentz force, Fermi surface effects etc., the anisotropic scattering due to spin-orbit interaction has been argued to be the main contributor to AMR^{39,40,41}. The anisotropic magnetoresistance in polycrystalline ferromagnets typically follows a $\cos^2\theta$ dependence, where θ is the angle between the current and magnetization vector of the sample.

This $\cos^2\theta$ type AMR in transition metal ferromagnets and alloys is understood theoretically through scattering of s-electrons in to empty d-states through spin-orbit interaction, $H_{SO} \approx \Delta_{SO}LS$, where L and S are orbital and spin angular momentum respectively and Δ_{SO} is the spin-orbit coupling parameter. In double exchange manganites the carrier lie in a band formed by itinerant e_g -band which is strongly coupled to localized t_{2g} band via strong Hund's coupling. Due to the itinerant nature of the e_g band the orbital moment ($L = 0$) is strongly quenched. However a small spin-orbit interaction of conduction carriers arises from the hybridized O 2p orbital. Moreover, in polycrystalline thin film of manganite the oxygen vacancy and deformations from ideal crystal structure at grain boundaries might result in an enhanced AMR⁴². The AMR at 3 kOe for two LSMO films of different texture is shown in Fig. 7. In case of the polycrystalline film deposited at 700 °C, the AMR can be fitted to an equation of the type $\text{AMR} (\%) = A + B \cos^2(\theta)$ with $A=2.94 \pm 0.03$ and $B=-2.98 \pm 0.05$. The $\cos^2\theta$ dependence reflects the spin-orbit coupling type AMR behavior. A more complicated functional behavior was found for the film deposited at 800 °C. Additional peaks were also found at $\theta = 60$, 120 and 180 degrees which can be attributed to pinning of the magnetization vector along certain direction in the plane of the film. Interestingly, the AMR

of these films is order of magnitude smaller than that of the polycrystalline films deposited at 700 °C. The larger AMR in case of polycrystalline samples may be understood in terms of stress fields at the grain boundaries. The strain at the grain boundaries may change intrinsic properties such as crystal-field splitting locally thereby affecting AMR amplitude drastically.

IV. CONCLUSIONS

We have presented a detailed study of magneto-transport in well characterized polycrystalline films of LSMO having different degrees of granularity and crystalline texture engineered by controlling the growth temperature. The granularity in films deposited at 700 and 800 °C was established through AFM imaging and $\theta - 2\theta$ X-ray diffraction. Although both the films showed ferromagnetic ordering at $T_C \approx 350$ K, the temperature dependence of the resistivity ($\rho(T)$) of these films was dramatically different. An order of magnitude higher resistivity, lower metal-insulator transition temperature and a low-temperature upturn of $\rho(T)$ was found in 700 °C deposited film because of the enhanced grain boundary scattering. A model for magnetotransport has been proposed by considering the film equivalent to a composite system of metallic LSMO granules embedded in a matrix of disordered metal

formed from oxygen deficient and strained LSMO at the grain boundaries. The temperature dependence of resistivity of this two-component composite is governed by the more resistive disordered metal which undergoes the double-exchange driven magnetic ordering and metallic transition at $T_P \approx 170$ K . At temperature below 50 K, an upturn in the resistivity is seen presumably due to a Kondo-type scattering from the Mn-spins at the grain boundaries. A large magnetoresistance (≈ 19 %) for a field of 0.3 T is seen at 10 K in films of $T_D = 700$ °C in comparison to only 0.4 % MR for 800 °C deposited films. The former also shows a two orders of magnitude higher anisotropic magnetoresistance. The dramatically different magnetotransport in such films presumably results from their two-component nature where spin-dependent scattering in the intergranular regions is dominant.

Acknowledgments

This research has been supported by grants from the Ministry of Communication and Information Technology (MCIT) and Board of Research in Nuclear Sciences (BRNS), Government of India. P. K. Muduli acknowledges financial support from the Council for Scientific and Industrial Research (CSIR), Government of India.

* Electronic address: rcb@iitk.ac.in

- ¹ G. Q. Gong, A. Gupta, G. Xiao, W. Qian, and V. P. Dravid, *Phys. Rev. B* **56**, 5096 (1997).
- ² J. M. D. Coey, A. E. Berkowitz, Ll. Balcells, F. F. Putris, and A. Barry, *Phys. Rev. Lett.* **80**, 3815 (1998).
- ³ H. Y. Hwang, S. W. Cheong, N. P. Ong, and B. Batlogg, *Phys. Rev. Lett.* **77**, 2041 (1996).
- ⁴ R. Shreekala, M. Rajeswari, K. Ghosh, A. Goyal, J. Y. Gu, C. Kwon, Z. Trajanovic, T. Boettcher, R. L. Greene, R. Ramesh, and T. Venkatesan, *Appl. Phys. Lett.* **71**, 282 (1997).
- ⁵ A. Gupta, G. Q. Gong, G. Xiao, P. R. Duncombe, P. Lecoeur, P. Trouilloud, Y. Y. Wang, V. P. Dravid, and J. Z. Sun, *Phys. Rev. B* **54**, R15629 (1996).
- ⁶ X. W. Li, A. Gupta, Gang Xiao, and G. Q. Gong, *Appl. Phys. Lett.* **71**, 1124 (1997).
- ⁷ K.-I. Kobayashi, T. Kimura, H. Sawada, K. Terakura, and Y. Tokura, *Nature (London)* **395**, 677 (1998).
- ⁸ D. D. Sarma, Sugata Ray, K. Tanaka, M. Kobayashi, A. Fujimori, P. Sanyal, H. R. Krishnamurthy, and C. Dasgupta, *Phys. Rev. Lett.* **98**, 157205 (2007).
- ⁹ D. Serrate, J M De Teresa, and M. R. Ibarra, *J. Phys.: Condens. Matter* **19**, 023201 (2007).
- ¹⁰ A. Milner, A. Gerber, B. Groisman, M. Karpovsky, and A. Gladkikh, *Phys. Rev. Lett.* **76**, 475 (1996).
- ¹¹ S. Lee, H. Y. Hwang, B. I. Shraiman, W. D. Ratcliff II, and S.-W. Cheong, *Phys. Rev. Lett.* **82**, 4508 (1999).
- ¹² L. I. Balcells, J. Fontcuberta, B. Martinez, and X. Obradors, *Phys. Rev. B* **58**, R14697 (1998).
- ¹³ M. García-Hernández, F. Guinea, A. de Andrés, J. L. Martínez, C. Prieto, and L. Vázquez, *Phys. Rev. B* **61**, 9549 (2000).
- ¹⁴ Sheng Ju, K. W. Yu, and Z. Y. Li, *Phys. Rev. B* **71**, 014416 (2005); **71**, 224401 (2005).
- ¹⁵ M. Ziese and S. P. Sena, *J. Phys.: Condens. Matter* **10**, 2727 (1998); M. Ziese, *Phys. Rev. B* **62**, 1044 (2000).
- ¹⁶ Jeng-Bang Yau, X. Hong, A. Posadas, C. H. Ahn, W. Gao, E. Altman, Y. Bason, L. Klein, M. Sidorov, and Z. Krivokapic, *J. App. Phys.* **102**, 103901 (2007).
- ¹⁷ J. ÓDonnell, J. N. Eckstein, M. S. Rzechowski, *Appl. Phys. Lett.* **76**, 218 (2000).
- ¹⁸ I. C. Infante, V. Laukhin, F. Sanchez, J. Fontcuberta, O. Melnikov, O. Yu Gorbenko, and A.

- R. Kaul, J. Appl. Phys. **99**, 08C502 (2006).
- ¹⁹ K. Senapati and R. C. Budhani, Phys. Rev. B **71**, 224507 (2005).
- ²⁰ Kyung-Ku Choi, T. Taniyama, and Y. Yamazaki, J. App. Phys. **90**, 6145 (2001).
- ²¹ Y. Tokura, Rep. Prog. Phys. **69**, 797 (2006).
- ²² M. B. Salamon and M. Jaime, Rev. Mod. Phys. **73**, 583 (2001).
- ²³ R. Bertacco, M. Riva, M. Cantoni, L. Signorini, and F. Ciccacci, Appl. Phys. Lett. **86**, 252502 (2005).
- ²⁴ G. Jeffrey Snyder, Ron Hiskes, Steve DiCarolis, M. R. Beasley and T. H. Geballe, Phys. Rev. B **53**, 14434 (1996).
- ²⁵ J. C. Chen, S. C. Law, L. C. Tung, C. C. Chi, and W. Guan, Phys. Rev. B **60**, 12143 (1999).
- ²⁶ K. Ghosh, C. J. Lobb, R. L. Greene, S. G. Karabashev, D. A. Shulyatev, A. A. Arsenov, and Y. Mukovskii, Phys. Rev. Lett. **81**, 4740 (1998).
- ²⁷ J.-H. Park, E. Vescovo, H.-J. Kim, C. Kwon, R. Ramesh, and T. Venkatesan, Nature (London) **392**, 794 (1998); Phys. Rev. Lett. **81**, 1953 (1998).
- ²⁸ R. Cauro, A. Gilabert, J. P. Contour, R. Lyonnet, M.-G. Medici, J.-C. Grenet, C. Leighton, and I. K. Shuller, Phys. Rev. B **63**, 174423 (2001).
- ²⁹ M. Ziese, Phys. Rev. B **60**, R738 (1999).
- ³⁰ P. Sheng and B. Abeles, Phys. Rev. Lett. **28**, 34 (1972).
- ³¹ B. Abeles, P. Sheng, M. D. Coutts, and Y. Arie, Adv. Phys. **24**, 407 (1975); B. Abeles, H. L. Pinch, and J. I. Gittleman, Phys. Rev. Lett. **35**, 247 (1975).
- ³² S. Honda, T. Okada, M. Nawate, and M. Tokumoto, Phys. Rev. B **56**, 14566 (1997).
- ³³ S. Kirkpatrick, Phys. Rev. Lett. **27**, 1722 (1971).
- ³⁴ S. Ju, H. Sun, and Z.-Y. Li, J. Phys.: Condens. Matter **14**, L631 (2002).
- ³⁵ O. Rapp, S. M. Bhagat and H. Gudmundsoon, Solid State Commun. **42**, 741 (1982).
- ³⁶ R. Hasegawa and C. C. Tsuei, Phys. Rev. B **2**, 1631 (1970); Phys. Rev. B **3**, 214 (1971).
- ³⁷ S. Mandal and R. C. Budhani, J. Magn. Magn. Mater. **320**, 3323 (2008).
- ³⁸ S. K. Bose, R. Sharma, and R. C. Budhani, Phys. Rev. B **78**, 115403 (2008).
- ³⁹ I. A. Campbell, A. Fert, and O. Jaoul, J. Phys. C **3**, S95 (1970).
- ⁴⁰ T. R. McGuire and R. I. Potter, IEEE Trans. Magn. **11**, 1018 (1975).
- ⁴¹ A. P. Malozemoff, Phys. Rev. B **32**, 6080 (1985).
- ⁴² R. Mathieu, P. Svedlindh, R. A. Chakalov, and Z. G. Ivanov, Phys. Rev. B **62**, 3333 (2000).

TABLE I: Fitting results of Eq. (1) and Eq. (9)

Film	ρ_1 ($\Omega\text{-cm}$)	A ($\Omega\text{-cm K}^{-2}$)	$A_{4.5}$ ($\Omega\text{-cm K}^{-4.5}$)
SrTiO ₃	1.1×10^{-4}	7.9×10^{-9}	4.3×10^{-15}
YSZ	2.2×10^{-4}	1.5×10^{-8}	6.2×10^{-15}
Field (T)	α ($\Omega\text{-cm}$)	δ ($\Omega\text{-cm K}^{-2}$)	γ ($\Omega\text{-cm}$)
0	8.3×10^{-1}	2×10^{-5}	-0.109
0.1	7.1×10^{-1}	2×10^{-5}	-0.089
0.2	6.6×10^{-1}	2×10^{-5}	-0.083
0.3	6.4×10^{-1}	2×10^{-5}	-0.078

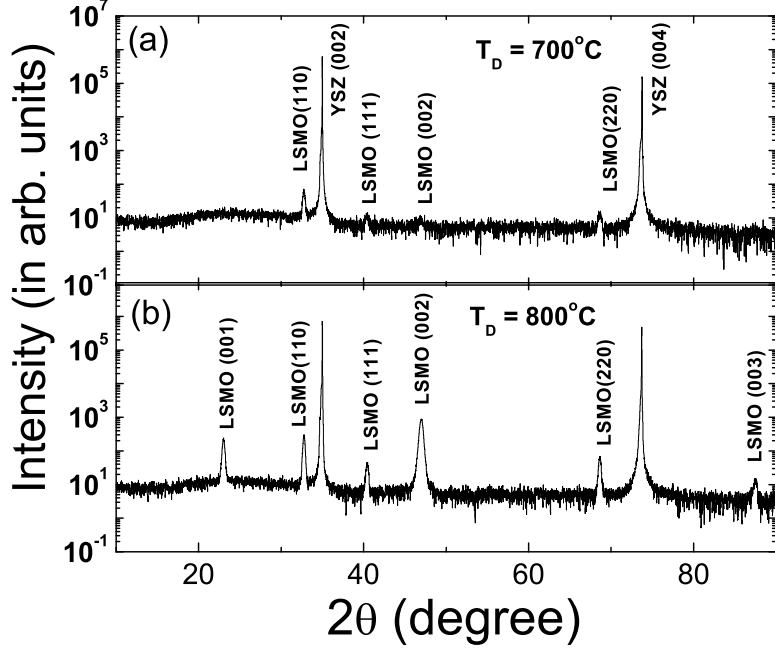


FIG. 1: (a,b) $\theta - 2\theta$ X-ray diffraction scans of 100 nm thick LSMO films deposited on (100) YSZ substrate at deposition temperature $T_D = 700^\circ\text{C}$ (a) and $T_D = 800^\circ\text{C}$ (b). The presence of (001), (hk0) and (hkl) reflections confirm a truly polycrystalline growth. All the orientations of LSMO thin film in this paper have been described in terms of pseudocubic unit cell.

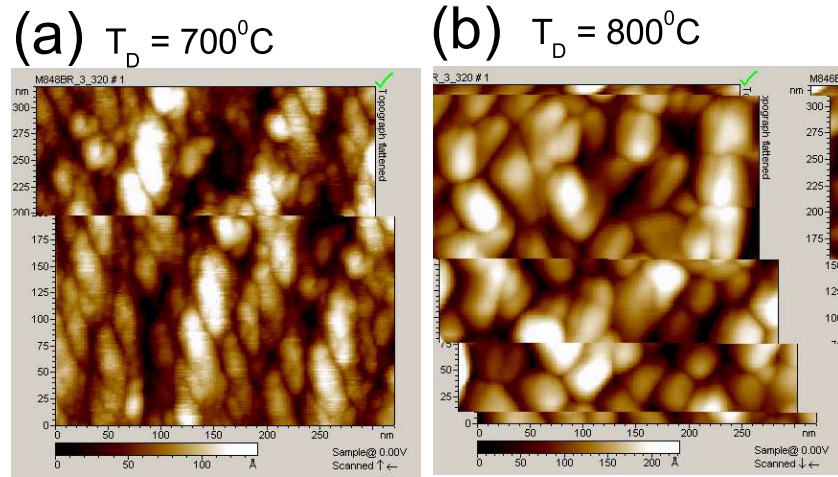


FIG. 2: (a,b) AFM photographs of 100 nm thick LSMO films deposited on (100) YSZ substrate at 700 and 800 $^\circ\text{C}$ are shown in panel 'a' and 'b' respectively. The images were taken at room temperature in non-contact mode.

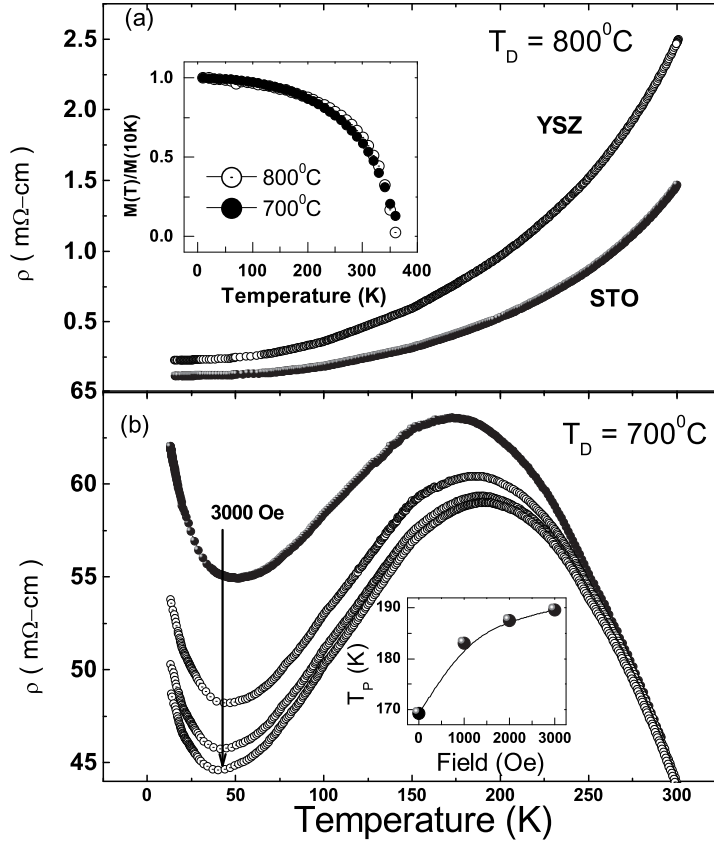


FIG. 3: (a) Temperature dependence of resistivity of a 100 nm thick LSMO film deposited at 800 $^{\circ}\text{C}$ on (100) YSZ and (100) STO substrates is shown in panel 'a'. The temperature dependence of field-cooled magnetization of the film on YSZ deposited at 700 and 800 $^{\circ}\text{C}$ is shown by closed and open circles respectively in the inset. Panel 'b' shows temperature and field dependence of resistance of a 100 nm thick LSMO film deposited at 700 $^{\circ}\text{C}$ on (100)YSZ. The inset shows the field- dependence of metal insulator-transition temperature T_P .

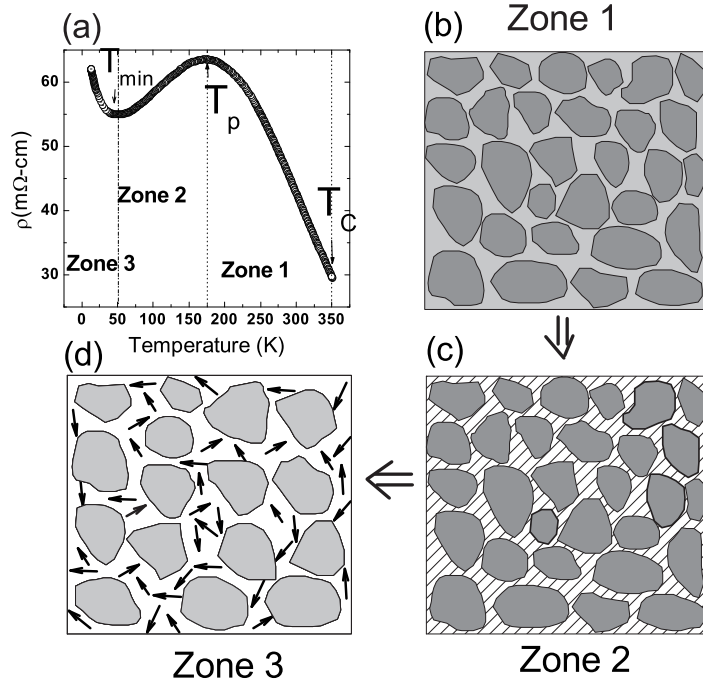


FIG. 4: Panel 'a' shows the zero-field resistivity of the 700 $^{\circ}\text{C}$ deposited polycrystalline film in the temperature range of 10 to 350 K. The curve has been divided into three temperature zones. Panel 'b', 'c' and 'd' are sketches of granular structure corresponding to Zone 1 to 3 respectively.

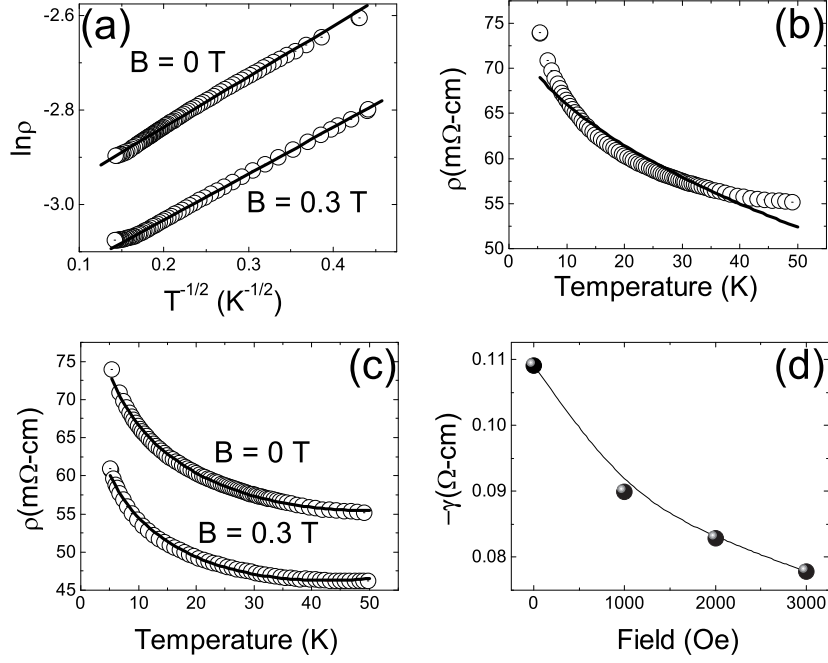


FIG. 5: Panel 'a' shows the $\exp [T^{-1/2}]$ dependence of the resistivity of a 100 nm thick polycrystalline film at $T \leq 50$ K for zero and 0.3 T field measurement. The solid line is a fit to the expression $\rho(T) \sim \exp\left(\frac{T_0}{T}\right)^{1/2}$. Panel 'b' and 'c' show the same data fitted to Eq. (5) and (7) of the text. The field dependence of coefficient γ of Kondo-type scattering found by fitting Eq. (7) to the data in Fig. 3(b) is shown in panel 'd'.

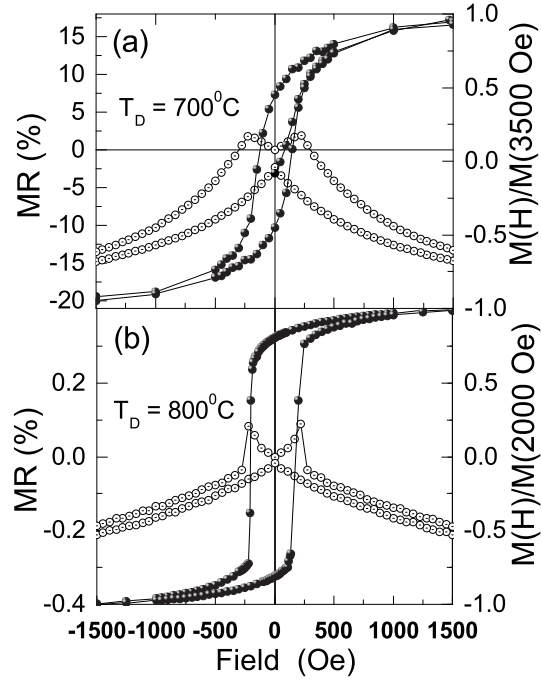


FIG. 6: Field dependence of magnetoresistance [$MR = \frac{R(H) - R(0)}{R(0)} \times 100$] at 20 K for LSMO films deposited at 700 and 800 °C is shown in panel 'a' and 'b' respectively. The field and current in these measurements are coplanar but orthogonal to each other. The $M(H)$ loops of the same film measured at 20 K in coplanar field are also shown.

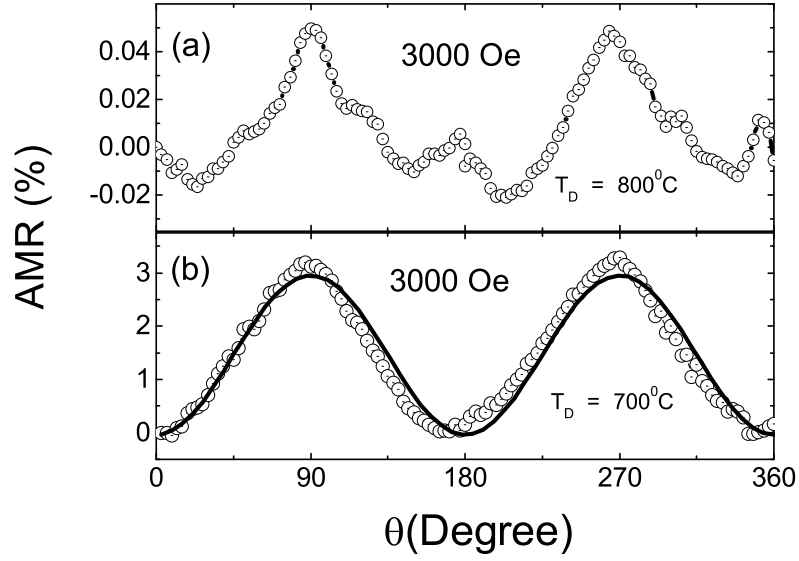


FIG. 7: Angular dependence of magnetoresistance (AMR) of two LSMO films measured at 50 K. Panels 'a' and 'b' are for the film deposited at 800 and 700°C respectively on YSZ(100) substrate. The angle θ is the angle between the applied magnetic field and the direction of current flowing through the sample. The field and current are coplanar. Solid line in the panel 'b' is a fit of the type $\text{AMR}(\%) \approx \cos^2\theta$.